Optical Materials 62 (2016) 553–560

Contents lists available at ScienceDirect

Optical Materials

journal homepage: www.elsevier.com/locate/optmat

Effect of Er^{3+} concentration on the luminescence properties of Al_2O_3-ZrO_2 powder

J.L. Clabel H. [a, *], V.A.G. Rivera [b], I.C. Nogueira [c], E.R. Leite [d], M. Siu Li [a], E. Marega Jr. [a]

[a] Instituto de Física de São Carlos, Universidade de São Paulo -USP, Caixa Postal 369, São Carlos, 13560-970, SP, Brazil
[b] Escuela de Física, Universidad Nacional Federico Villarreal - UNFV, Lima-Lima, Perú
[c] Departamento de Física, Universidade Federal do Amazonas - UFAM, Manaus, 69077-000, AM, Brazil
[d] Departamento de Química, Universidade Federal de São Carlos -UFSCar, Caixa Postal 676, São Carlos, 13565-905, SP, Brazil

ARTICLE INFO

Article history:
Received 3 September 2016
Received in revised form
22 October 2016
Accepted 12 November 2016
Available online 23 November 2016

Keywords:
Luminescence
Erbium
Crystallization phases
Lifetime

ABSTRACT

This manuscript reports on the effects of the luminescence properties of Er^{3+} on Al_2O_3-ZrO_2 powder synthesized by the conventional solid-state method. The best conditions found for the calcinations were 1500 °C and 4 h. The structural dependence of the luminescence on Er^{3+}:Al_2O_3-ZrO_2 is associated with phase transformations of the Al_2O_3-ZrO_2 host and presence of the OH group. Green and red emissions at room temperature from the $^2H_{11/2}$, $^4S_{3/2} \rightarrow {}^4I_{15/2}$ and $^4F_{9/2} \rightarrow {}^4I_{15/2}$ levels of Er^{3+} ions were observed under 482 nm pumping. The green-to-red emission intensity ratios and CIE chromaticity coordinates were determined from emission spectra for the evaluation of light emitted as a function of the Er^{3+} concentration. The Er^{3+} luminescence quenching due to group OH and variation in the Er^{3+} concentration plays an important role in the definition of the luminescent response.

1. Introduction

The luminescence of rare earth in a solid state matrix is of great interest because of its promising high-performance photonic applications [1,2]. The Erbium ion (Er^{3+}) has been widely studied due to its multicolor tunability from the transition probabilities [3–5]. Materials with lower phonon energy can effectively restrain the multi-phonon relaxation of the energy level and Al_2O_3-ZrO_2 powder has emerged as a candidate due to its good mechanical properties, microstructure stability and lower phonon energy [6–8]. In contrast, little attention has been paid to its optical properties in Al_2O_3-ZrO_2 systems at different Er^{3+} concentrations. F.F. Lange [9] studied the formation of the Al_2O_3-ZrO_2 system from the reaction between Al_2O_3 and ZrO_2 at 1500 °C. The author analyzed the effect of the reactions conditions on the crystal structure and observed the tetragonal phase of ZrO_2 could be retained in volume fractions of up to 20%. As Al_2O_3-ZrO_2 exhibits such characteristic, it could be a potential host for harvesting visible light. Er^{3+} ions in the host Al_2O_3-ZrO_2 composite have attracted interest due to their possible application in visible and near-infrared regions. Their local environment can provide a surrounding for the coexistence of Er, and optically activate Er^{3+} ions [10]. Therefore, Er_2O_3 can be a promising complement to the Al_2O_3-ZrO_2 composite due to the f-f transitions within the $4f^{11}$ electronic shell of Er^{3+} ions, i.e., $^4F_{9/2}$, $^2H_{11/2}$ and $^4S_{3/2}$ for ground state $^2I_{15/2}$ [11,12]. Such transitions occur when Er^{3+} ions occupy a lattice site of no inversion symmetry and are associated with electric dipole. Conversely, the electric dipole emission is forbidden when occupies a site of inversion symmetry. In this sense, the analysis of the luminescence emission of Er^{3+} ions in the host Al_2O_3-ZrO_2 enables the understanding of the luminescence properties that change in response to the variation in both Er^{3+} concentration and Al_2O_3/ZrO_2 ratio, from fundamental and technological viewpoints.

This paper reports on the emission of Er^{3+} ions in the host Al_2O_3-ZrO_2 composite under 482 nm laser excitation, from down-conversion processes. Samples were prepared with different Er^{3+} concentrations and Al_2O_3/ZrO_2 ratio and both intensities and lifetime of the down-conversion were evaluated for the distinction and improvement of the intensity of Er^{3+} ions emissions. Structural and functional group analyses by X-ray diffraction and infrared spectroscopy, respectively, were also discussed. Such emissions by down conversion are a result of the phase transformation from monoclinic to tetragonal phases due to the Er^{3+} concentration and surface defects.

* Corresponding author.
E-mail address: jclabel@ifsc.usp.br (J.L. Clabel H.).

http://dx.doi.org/10.1016/j.optmat.2016.11.020
0925-3467/

2. Experimental procedure

Er^{3+} on Al_2O_3-ZrO_2 powder was synthesized by the conventional solid-state reaction method (SSR). Precursor ZrO_2 (Aldrich, 99.8%), Er_2O_3 (Aldrich, 99.8%) and Al_2O_3 (J.T. Baker, 98%) oxides were weighed according to the desired stoichiometric and mixed in a ball mill with isopropyl alcohol as solvent and zirconium oxide balls as the milling medium for 20 h. The molar compositions chosen and the result of the phase analysis after calcination for an annealed temperature of 1500 °C are shown in Table 1. Initially, an analysis of the influence of temperature on the luminescence was conducted for sample E5A5. E5A5 powder was treated at 700–1500 °C temperatures for 4 h. After the thermal treatment, the sample was analyzed by X-ray powder diffraction and luminescence, Fig. 1(a–b). The annealing temperature (1500 °C) was chosen for samples with different Er^{3+} concentrations, according to the maximum response of the luminescence intensity observed for E5A5 sample, Fig. 1(b).

Er^{3+} on Al_2O_3-ZrO_2 powder was characterized by X-ray powder diffraction (XRD) on a Rigaku Dmax 2500 PC diffractometer of CuK_α radiation in an angular range between 10° and 75°, 2° min^{-1} scanning velocity and 0.02° step size. An SEM/EDS instrument (Model XL-30, Philips, Japan) operated at 25 kV determined the morphology and composition of Er^{3+} on Al_2O_3-ZrO_2 powder. Infrared (IR) measurements were taken in a Fourier transform infrared (FTIR) spectrometer (Model: PerkinElmer Make: Spectrum RX I) for investigations of OH, Zr-O, and Al-O absorption bands in the 2500–10000 nm range and luminescence measurements were performed in a Thermo Jarrel-Ash Monospec 27 monochromator and a Hamamatsu R446 photomultiplier with a data acquisition system controlled by a microcomputer. The excitation source was a 482 nm laser diode of 500 mW. The effective lifetime of the $^4S_{3/2}/^2H_{11/2}$ and $^4F_{9/2}$ levels for the $^4I_{15/2}$ ground state following direct excitation at 567 nm and 683 nm with 1 00 ns pulse width was measured by a chopper (Stanford) with a monochromator and lens connected to a Tektronix digital oscilloscope (TDS 380). The lifetime was calculated by $I(t)=I_0e^{-t/\tau}$, where I_0 is the intensity at time zero. All measurements were performed at room temperature and under 482 nm excitation.

3. Results and discussion

Fig. 1(a) shows E5A5 powder calcined at 700–1500 °C temperatures. The annealed temperature controls the particle growth; likewise, the crystalline structures depend on the particle size and thermodynamic stability [13]. The effect of particle size on the luminescence from annealing Er^{3+}/Yb^{3+} co-doped Al_2O_3-ZrO_2 powders was experimentally observed by Q. Ding et al. [14] At temperatures above 900 °C, the particle size is expected to increase and the surface area decreases due to the particle growth [13]. The luminescence properties of Er^{3+} on Al_2O_3-ZrO_2 powder (sample E5A5) were investigated at a 482 nm excitation wavelength. The Er^{3+} emission on Al_2O_3-ZrO_2 powder (Fig. 1(b)) strongly depends on the annealing temperature. The XRD pattern illustrated in Fig. 1(a) reveal that the diffraction peaks for the E5A5 powders present two phases that can be indexed to the tetragonal structure with space group P42/nmc for the ZrO_2 phase (named t-ZrO_2) which is in agreement with the Inorganic Crystal Structure Database (ICSD No. 66781) [15] and to the monoclinic structure with space group P121/c1 for the ZrO_2 phase (named m-ZrO_2) which is in agreement with the ICSD No. 18190 [16]. No other phase was observed, indicating that there was an incorporation of Al^{3+} and Er^{3+} ions in the t-ZrO_2 and m-ZrO_2 structures. At low annealing temperatures (700 °C), the monoclinic phase (low-symmetry) is dominant, whereas at a higher temperature (1500 °C), the tetragonal phase is dominant (high-symmetry). Such results indicate the concentration of Er^{3+} on Al_2O_3-ZrO_2 powder in combination with higher annealing temperatures leads to a significant improvement in Er^{3+} on Al_2O_3-ZrO_2 powder luminescence (Fig. 1(b)). The luminescence intensity drastically increases in function of increases in the particle size and changes in the phases. Likewise, when the Er^{3+} ion occupies a lattice site of low-symmetry, the transition probabilities of Er^{3+} ions in Al_2O_3-ZrO_2 powder decrease. The low symmetry can be interpreted from electronic states inside band gap due to the creation of point-defects (oxygen vacancies), enriched with Al/Zr or impurity on the surface of the particles [17].

The larger response of the luminescence intensity at high annealing temperatures induces a systematic study of Er^{3+} on Al_2O_3-ZrO_2 powder at different Er^{3+} concentrations. The effect of Er^{3+} concentration and phase transformation on the luminescence intensity was investigated for improvements in the luminescence efficiency in Er^{3+} on Al_2O_3-ZrO_2 powder.

The XRD patterns of the powders annealed at 1500 °C for 4 h are shown in Fig. 2(a–d). It was observed the presence of both tetragonal ZrO_2 (t-ZrO_2) and monoclinic ZrO_2 (m-ZrO_2) phases in Er^{3+} on Al_2O_3-ZrO_2 powders. The (−111), (111) and (101), (110) plans correspond to the m-ZrO_2 and metastable t-ZrO_2 phases, respectively. No other phase was observed, indicating that there was an incorporation of Al^{3+} and Er^{3+} ions in the t-ZrO_2 and m-ZrO_2 crystal lattices. To check the incorporation of ions was performed Rietveld refinement of two compositions studied (E3A5 and E5A10). The Rietveld refinements were performed through the general structure analysis (GSAS) program [18]. The measured diffraction patterns are well adjusted to the ICSD No. 66781 [15] and No. 18190 [16]. Fig. 3 shows Rietveld refinement plots for E3A5 and E5A10 compositions. The differences between the XRD pattern profiles observed experimentally and the theoretically calculated data are near to zero in the intensity scale, as illustrated by the line Yobs-Ycalc. Table 2 shows low deviations of the statistical parameters R_{wp}, R_p, R_{Bragg} and χ^2, which indicate the good quality of the structural refinements and the numerical results. Structural refinement data confirm that E3A5 and E5A10 powders are crystallized in the t-ZrO_2 and m-ZrO_2 structures, and there is no other additional phase. Further, in Table 2 shows the quantification of the phases present and Table 3 shows the lattice parameters and unit-cell volume for each phase. All results are in agreement with reports in the literature for ZrO_2 phase [12,19].

The concentration of each phase depends on the Er^{3+} ion concentration. The higher the concentration of the ion Er^{3+}, the t-ZrO_2 phase is dominant. The phase changes observed are partially due to the difference in the ionic radii of the constituents, as well as the charge compensation by the difference of valence [20]. Zr^{4+} ion has

Table 1
Notation of the samples and phase composition after annealing at 1500 °C.

Sample	x(ZrO_2)	y(Er_2O_3)	z(Al_2O_3)	Phase Present
				1500 °C
E3A5	0.92	0.03	0.05	t-ZrO_2+m-ZrO_2
E3A10	0.87	0.03	0.10	t-ZrO_2+m-ZrO_2
E3A15	0.82	0.03	0.15	t-ZrO_2+m-ZrO_2
E5A5	0.90	0.05	0.05	t-ZrO_2+m-ZrO_2
E5A10	0.85	0.05	0.10	t-ZrO_2+m-ZrO_2
E5A15	0.80	0.05	0.15	t-ZrO_2+m-ZrO_2
E7A5	0.88	0.07	0.05	t-ZrO_2+m-ZrO_2
E7A10	0.83	0.07	0.10	t-ZrO_2+m-ZrO_2
E7A15	0.78	0.07	0.15	t-ZrO_2+m-ZrO_2
E10A5	0.85	0.10	0.05	t-ZrO_2 +m-ZrO_2
E10A10	0.80	0.10	0.10	t-ZrO_2+m-ZrO_2
E10A15	0.75	0.10	0.15	t-ZrO_2 +m-ZrO_2

m = monoclinic t = tetragonal.

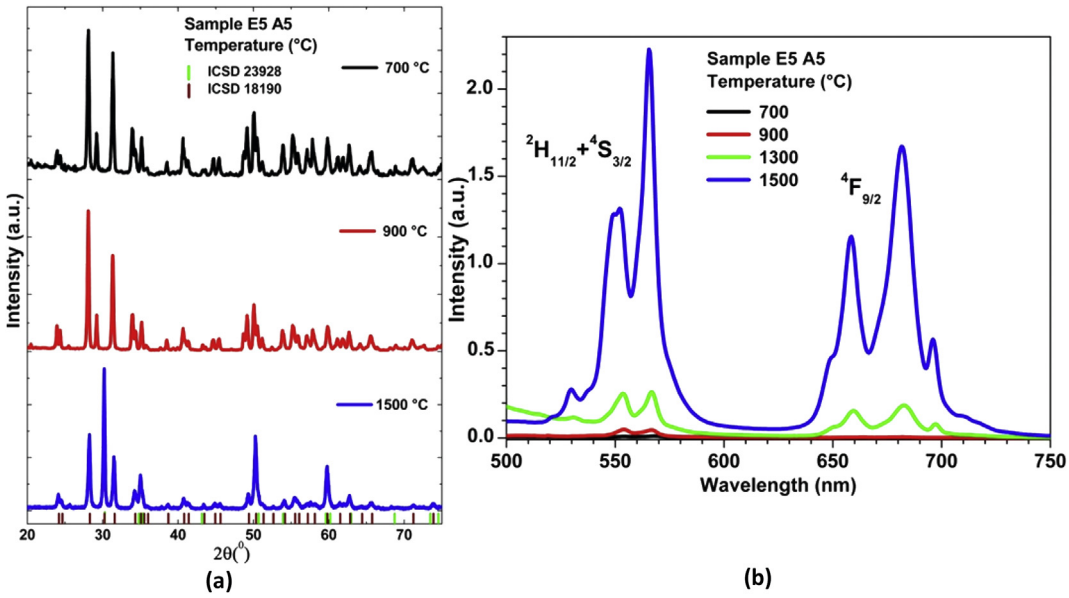

Fig. 1. (a) XRD spectra of the powder annealed at 700–1500 °C temperatures for 4 h. (b) Photoluminescence spectra of Er^{3+} on Al_2O_3-ZrO_2 powder at different temperatures and under 482 nm laser excitation.

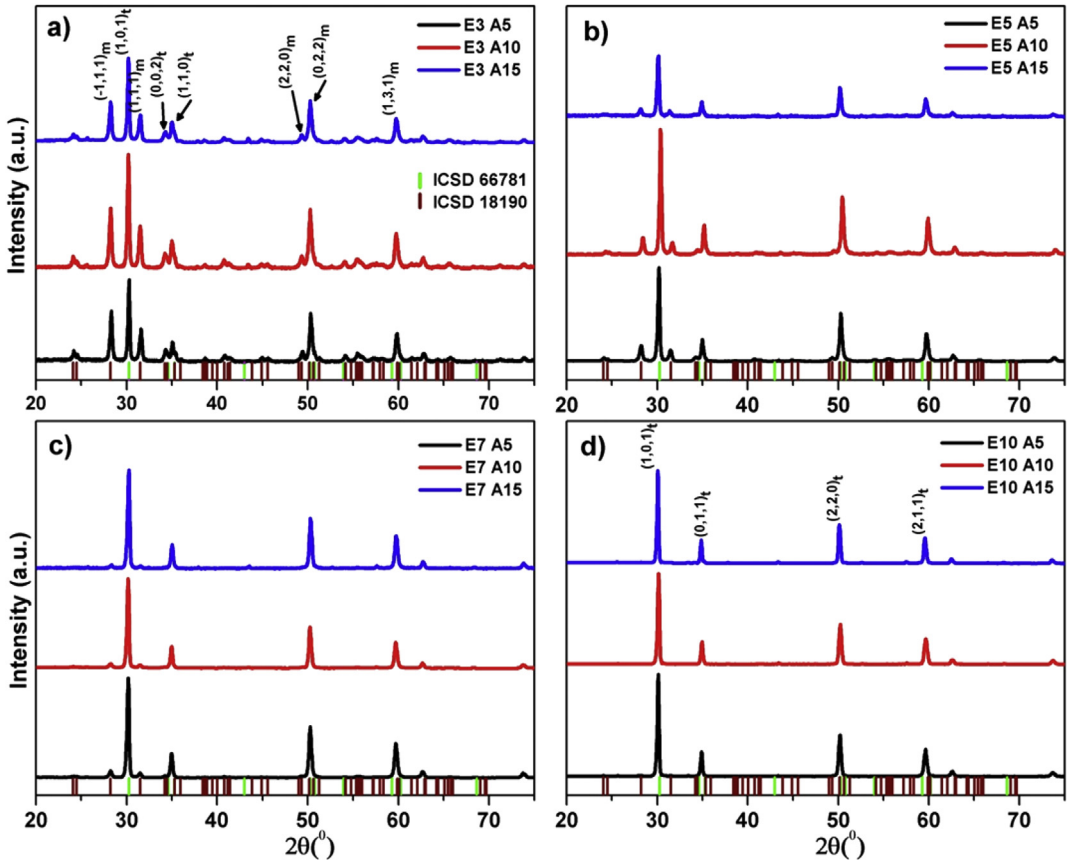

Fig. 2. XRD spectra of the powder annealed at 1500 °C for 4 h.

sevenfold coordination and eightfold coordination with oxygen ions in monoclinic and tetragonal phases, respectively [21]. The increase in the Er^{3+} ion concentration leads to a phase change and Al^{3+} ions contribute to the stabilization phase. Therefore, the monoclinic phase (at low Er^{3+} concentrations) is less symmetric than the tetragonal phase (at high Er^{3+} concentrations) and the low site symmetry in the Al_2O_3-ZrO_2 powder increases the transition probabilities of Er^{3+} ions from $^2H_{11/2}/^4S_{3/2}$ and $^4F_{9/2}$ levels to the $^4I_{15/2}$ ground state.

The SEM images show the particles size distribution of Er^{3+} on

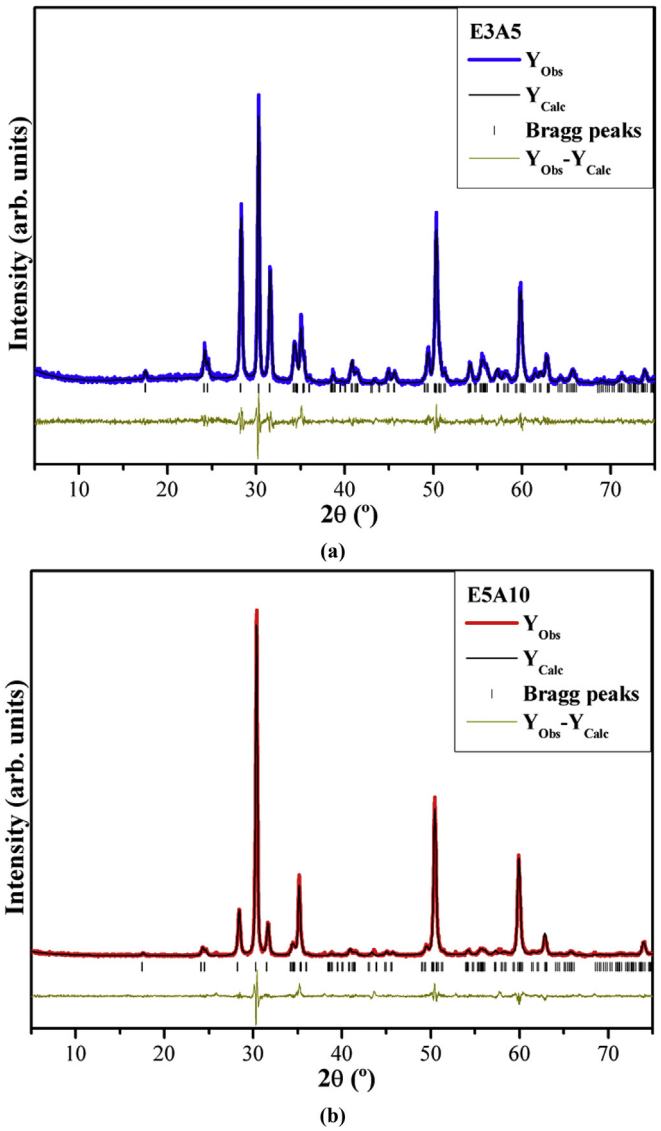

Fig. 3. Rietveld refinement for the E3A5 and E5A10 powders annealed at 1500 °C for 4 h.

Table 2
Quantification of the phases and statistical parameters of quality obtained by Rietveld refinement for the E3A5 and E5A10 powders annealed at 1500 °C for 4 h.

Samples	t - ZrO_2 (%)	m - ZrO_2 (%)	χ^2	R_{Bragg}	R_p	R_{wp}
E3A5	37.31	62.69	1.26	5.81	9.80	12.68
E5A10	70.45	29.55	1.43	5.95	9.85	13.42

Al_2O_3-ZrO_2 powder in E3A15, E5A15, E7A15 and E10A15, Fig. 4(a–d). The microstructures of the ceramic powder annealed at 1500 °C for 4 h indicate the formation of particles of 0.7–2.0 μm average size, Fig. 4(a–c). The high concentration of microparticles revealed to an irregular morphologies, which causes a non-uniform particle size distribution. The Al_2O_3-ZrO_2 powder microstructure is affected at high concentrations of Er^{3+} ions (E10A15), Fig. 4(d), which leads to particle sizes smaller than 1.0 μm. According to the literature [22,23], the substitution of Er^{3+} and Al^{3+} ions in ZrO_2 slightly increases the particle size and improves the luminescence performance in ZrO_2. The EDX data are used for the qualitative elemental analysis in Er^{3+} on Al_2O_3-ZrO_2 powder to indicate the elements present and their relative abundance. The chemical composition of the EDX spectrum of Er^{3+} on Al_2O_3-ZrO_2, shown in Fig. 5, confirmed the presence of Zr, Er, Al and O in the sample. Spectra taken at selected positions show the presence of the same constituents. Fig. 5 displays the chemical composition (at. %) of the Er^{3+} elements on Al_2O_3-ZrO_2 powder for each compound formed from EDX. The high concentrations of oxygen atoms revealed the adsorption in Er^{3+} on Al_2O_3-ZrO_2 powder annealed at 1500 °C for 4 h. Such an oxygen increase may decrease the luminescence emission intensity of Er^{3+} on Al_2O_3-ZrO_2 powder.

The FTIR spectra data shown in Fig. 6 were obtained from a mixture in potassium bromide (KBr). They exhibit three distinct broad bands corresponding to ~2900, ~4200 and ~6300 nm. The first band is generally attributed to adsorbed water and/or OH stretching vibration (2900–3333 nm range) [24,25]. The decrease in the band intensity OH in Er^{3+} on Al_2O_3-ZrO_2 powder can be ascribed to the increase in the Er^{3+} concentration. The absorption bands of OH became weaker when the concentrations of Er^{3+} ions in Al_2O_3-ZrO_2 powder were 7 and 10 mol%. The significant reduction of the OH group may be related to the increase of the crystal field symmetry around Er^{3+}. Such a high-symmetry is achieved from samples at high concentrations of Er^{3+} ions (7 and 10%) [26]. Small bands are associated with CH and CH_3 groups at 3390 and 3457 nm [27]. The second band at ~4200 nm is attributed to the formation of erbium hydroxide (Er-OH) and aluminum hydroxide (Al-OH), which show a slight variation as a function of the Al^{3+}:Er^{3+} concentrations. Besides, the Er^{3+} efficiency can be affected by the presence of the OH group, which might induce a transfer of energy from the $^2H_{11/2}/^4S_{3/2}$ and $^4F_{9/2}$ levels to the OH bond. The decrease in the peak intensity at 4200 nm can be interpreted as the breakage of the Er–OH, Al–OH bonds and cation field strength of Zr^{4+} in the structure. V. Rivera et al. [28] reported the spectra between 4150 and 4400 cm^{-1} are attributed to the atmospheric carbon dioxide adsorbed on the sample surface. Asymmetric and symmetric C=O stretching modes of Er^{3+} on Al_2O_3-ZrO_2 powder were observed at ~6200 nm. The most notable change in the spectrum occurred in samples with increasing Er^{3+} concentrations (7 and 10 mol%), where the bands at ~2756, ~3010 and ~6000 cm^{-1} were suppressed and gradually decreased due to the removal of free and combined water from the sample after a thermal treatment.

Fig. 7(a–d) show the luminescence spectra obtained from 520 nm up to 720 nm, which correspond to $^2H_{11/2}/^4S_{3/2}$, $^4F_{9/2}$ and

Table 3
Lattice parameters and unit cell volume obtained by Rietveld refinement for the E3A5 and E5A10 powders annealed at 1500 °C for 4 h.

Samples	t - ZrO_2			m - ZrO_2			
	Lattice Parameters (A)		Volume (A^3)	Lattice Parameters (A)			Volume (A^3)
	a = b	c		a	b	c	
E3A5	3.632(5)	5.133(8)	67.742(6)	5.158(5)	5.210(3)	5.315(6)	141.034(1)
E5A10	3.631(3)	5.139(9)	67.779(1)	5.162(1)	5.211(1)	5.315(3)	141.172(2)

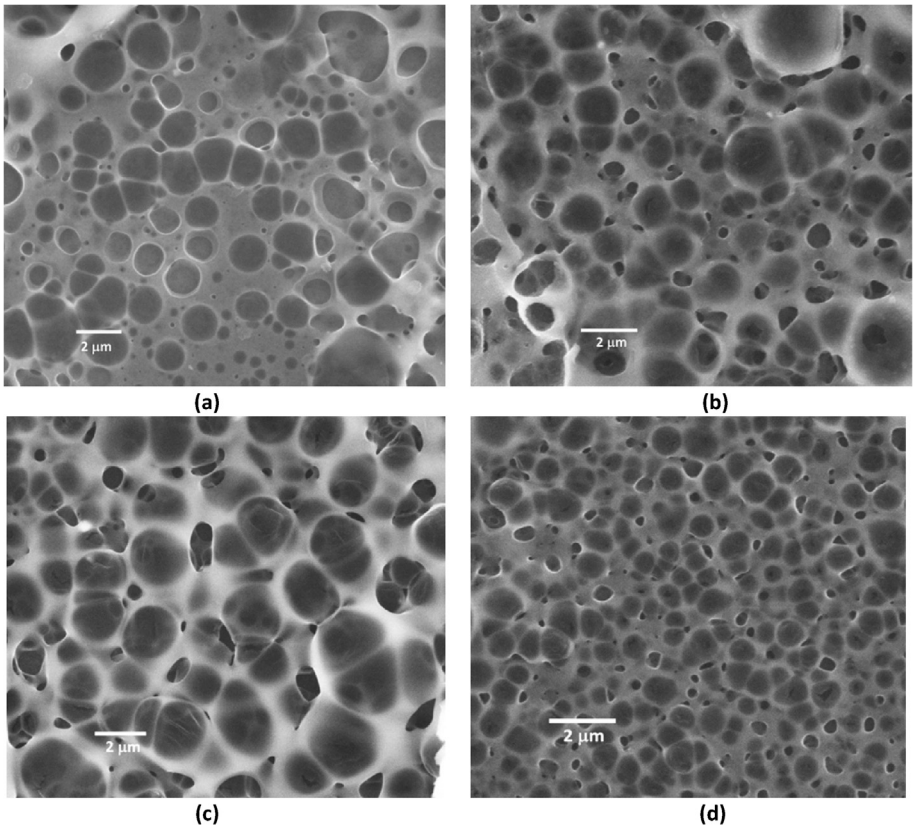

Fig. 4. SEM images of Er^{3+} on Al_2O_3-ZrO_2 powder annealed at 1500 °C for different Erbium concentrations: a) E3A15, b) E5A15, c) E7A15 and d) E10A15.

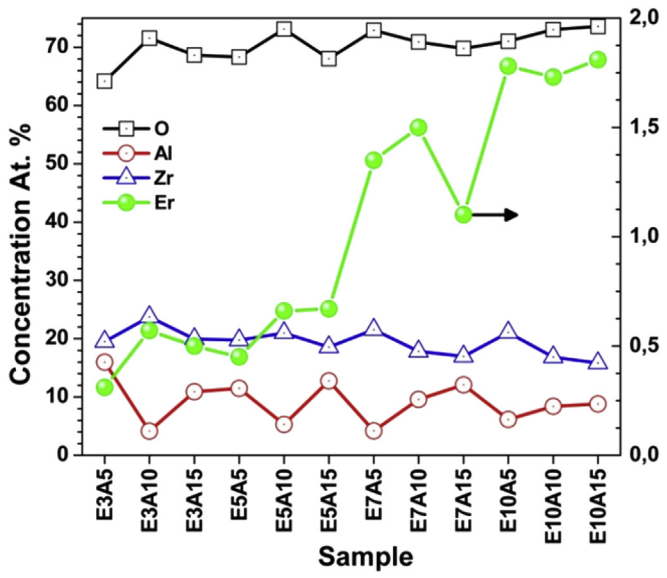

Fig. 5. Chemical EDX composition of constituent elements O, Al, Zr and Er of the samples studied.

$^4I_{9/2}$ transitions to the ground state $^2I_{15/2}$ of the Er^{3+} ion, when excited at 482 nm. Such emissions in the luminescence spectra suggest the local environment of Er^{3+} ion is affected by the phase mixture, evidenced by the XRD patterns. The luminescence efficiency at Er^{3+}:Al_2O_3-ZrO_2 is dependent on the concentration variation of Er^{3+} and crystalline phase of the host materials. The following characteristics can be summarized: when the Er^{3+} concentration is low (3 and 5 mol % Er_2O_3), the interaction between Er^{3+} ions can be neglected, however, the non-radiative processes contribute to an easier transition of the $^4F_{7/2} \rightarrow {}^4S_{3/2}$ level than that for the $^4F_{9/2}$ level, which justifies why green emissions are stronger than red emissions. The increase in the Er^{3+} concentration (7 and 10 mol % Er_2O_3) induces a favorable process due to the interaction between Er^{3+} ions. During this process, the Er^{3+} ions in the $^4F_{7/2}$ level decay non-radiatively to the $^4S_{3/2}/^2H_{11/2}$ level and benefit the transition to the $^4F_{9/2}$ level, rather than to the $^4S_{3/2}$ level, which results in a decrease in the green emissions and increase in the red emissions. On the other hand, the variation in the luminescence efficiency might also be attributed to the divergence of the local environment surrounding Er^{3+} ions and surface defects in the particles of the host material. The surface is responsible for non-radiative energy transfers from the $^2H_{11/2}/^4S_{3/2}$ level of the Er^{3+} ions to the O-H vibrations. R.I. Merino et al. [29] reported the drop luminescence intensity is associated with surface defects and symmetry distortions, since their optical properties depend on their environment. No significant changes were observed in the luminescence spectra when the Er^{3+} concentrations were fixed and the Al^{3+} concentration increased. Nevertheless, the near-infrared emission intensity is weak and constant for all samples, as shown in the inset of Fig. 7(a–d), and can be explained by the energy level diagram of Er^{3+}, Fig. 8(a). As the host matrix has a mixed phase (monoclinic and tetragonal) rather than a cubic structure, the transition selection rules of Er^{3+} are relaxed, consequently, the Er^{3+} emission can be observed. The laser light directs the Er^{3+} ion to the $^4F_{7/2}$ level, and the non-radiatively excited $^4F_{7/2}$ level decays to the $^2H_{11/2}/^4S_{3/2}$ and $^4F_{9/2}$ levels. A radiative relaxation process of Er^{3+} ions in the $^2H_{11/2}/^4S_{3/2}$ and $^4F_{9/2}$ levels for ground state $^4I_{15/2}$ occurs and produces the red and green emissions. The populations of the $^2H_{11/2}$ and $^4S_{3/2}$ levels are linearly proportional to the Er^{3+}

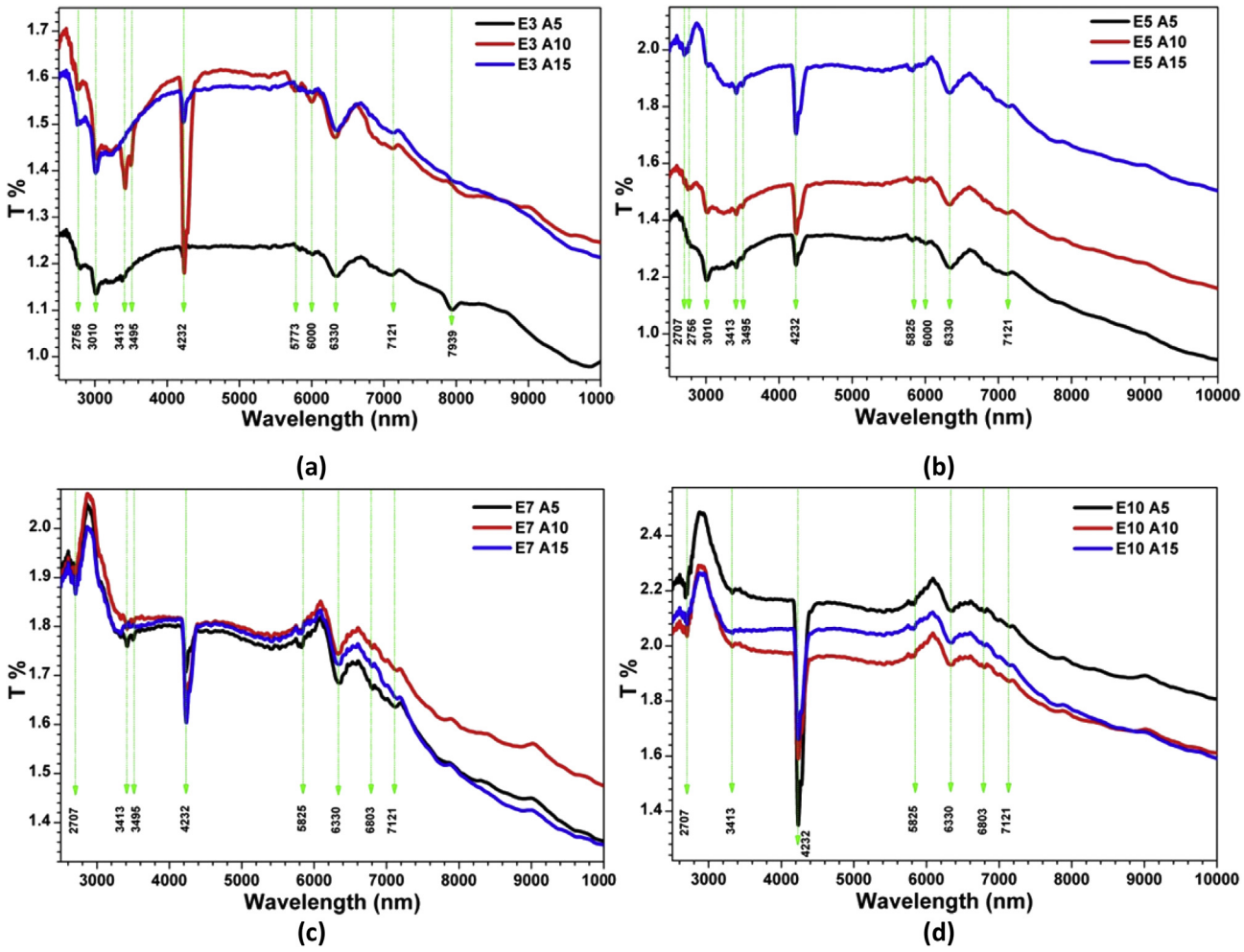

Fig. 6. FT-IR analyses of the powder annealed at 1500 °C for 4 h.

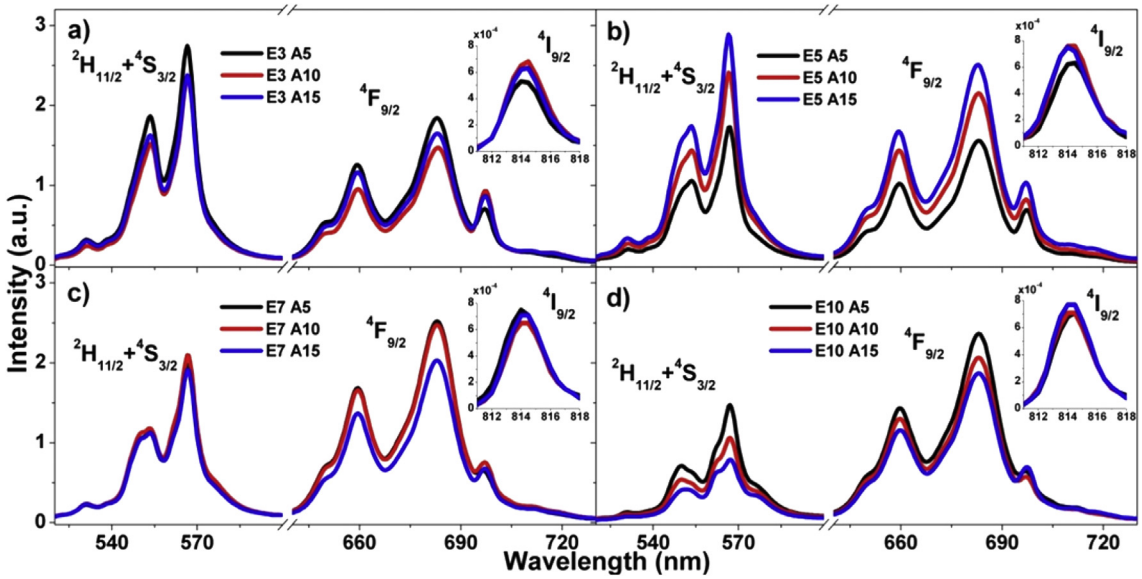

Fig. 7. Photoluminescence spectra of the powder prepared for mixture oxides excited at 482 nm.

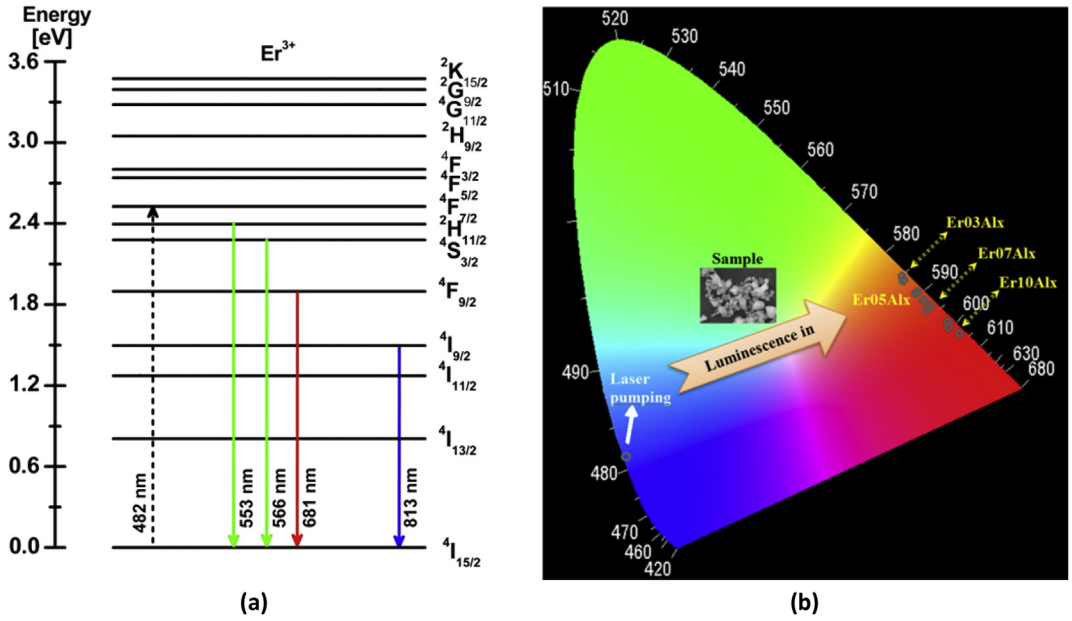

Fig. 8. (a) Diagram of the energy level of Er^{3+} in the Al_2O_3-ZrO_2 system indicating down-conversion and CR mechanism under 482 nm excitation. (b) CIE-1931 chromaticity for Er^{3+} on Al_2O_3-ZrO_2 powder.

concentration, therefore, if the Er^{3+} concentration is low, the interaction between Er^{3+} ions can be neglected. Moreover, the characteristic emission band of the $^4I_{9/2}$ level relaxes radiatively to the ground state ($^4I_{15/2}$) of the Er^{3+} ion followed by non-radiatively transitions, which promotes emissions in 814 nm through the $^4I_{9/2} \rightarrow {}^4I_{15/2}$ transitions. P. Jenouvrier et al. and Z. Chen et al. reported such a behavior can be associated with the Stark level split of Er^{3+} ions $^4I_{9/2} \rightarrow {}^4I_{15/2}$ in the crystalline host [30,31]. The diagram constructed by the Commission Internationale de l'Eclairage (CIE) chromaticity for Er^{3+} on Al_2O_3-ZrO_2 was calculated by luminescence emission spectra using the energy distribution. According to the diagram in Fig. 8, the tuning of the orange to green emissions is dependent only on the Er^{3+} concentration.

The effect of the Er^{3+} concentration upon the luminescent lifetime of the $^4S_{3/2}$ (567 nm) and $^4F_{9/2}$ (683 nm) levels under 482 nm excitation is shown in Fig. 9 for the sample with Er^{3+} (3 mol %) concentrations. The decay after 482 nm excitation can be described by a single exponential function. A similar behavior is observed for all concentrations. The proposed cross relaxation mechanisms are supported by measurements of Er^{3+} lifetime decays of the $^4S_{3/2}$ and $^4F_{9/2}$ levels. As shown in Table 4, the lifetime values ranged between 120.0 and 153.3 μs and 140.7 and 172.7 μs, respectively, and were higher than the value reported by G. Maciel et al. [23] for Er^{3+} doped ZrO_2. The decrease in the lifetime at 567 nm with the increase in the Er^{3+} concentration (3 and 5 mol %) and Al_2O_3/ZrO_2 ratio of 153.3 to 130.2 μs can be due to two mechanisms, namely (1) quenching effect, present at low concentrations, and (2) effect of impurities related to energy transfers of the $^2H_{11/2}/{}^4S_{3/2}$ level to the O-H vibrations. However, for high Er^{3+} (7 and 10 mol %) concentrations, the lifetime increases from 125.6 to 153.3 μs, which indicates the effect of impurities is negligible when the Al_2O_3/ZrO_2 ratio decreases. In contrast, for the red emission from the $^4F_{9/2}$ level, the lifetime is longer (for low concentration), which indicates the energy transfer process is higher than that for the $^4S_{3/2}$ level. The

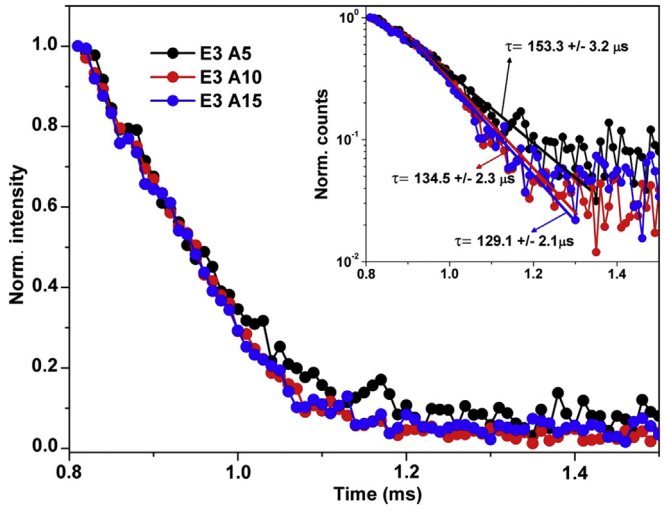

Fig. 9. Normalized luminescence decay of the 567 nm emission band under excitation at 482 nm. Inset shows lifetime fits, showing decay contributions with lifetimes of τ = 153.3 μs(E3 A5), τ = 134.5 μs(E3 A10) and τ = 129.1 μs(E3 A15).

Table 4
Lifetimes of the $^4S_{3/2}$ and $^4F_{9/2}$ levels obtained under excitation at 482 nm at room temperature. (λ_{em} is the emission wavelength).

λ_{ex} = 482 nm		
Samples	λ_{em} = 567 nm	λ_{em} = 683 nm
	τ ($^4S_{3/2}$) (μs)	τ ($^4F_{9/2}$) (μs)
E3A5	153.3 ± 3.2	172.7 ± 1.9
E3A10	134.5 ± 2.3	148.9 ± 1.6
E3A15	129.1 ± 2.1	154.1 ± 2.2
E5A5	135.0 ± 2.2	144.5 ± 1.8
E5A10	131.8 ± 2.1	141.1 ± 2.3
E5A15	130.2 ± 1.8	140.7 ± 2.3
E7A5	125.6 ± 1.8	167.3 ± 2.1
E7A10	136.5 ± 2.3	151.4 ± 1.8
E7A15	142.2 ± 2.5	145.0 ± 1.6
E10A5	120.0 ± 1.6	145.8 ± 1.4
E10A10	127.4 ± 1.6	147.2 ± 1.9
E10A15	153.3 ± 1.7	159.1 ± 1.8

further increase in the Er^{3+} concentration leads to a 167.3 to 145.0 μs reduction in the $^4F_{9/2}$ lifetime, which explains the dependence of the spectra intensity distribution between the green and red emission bands on the Er^{3+} concentration and surface defects (when the Al_2O_3/ZrO_2 ratio decreases).

4. Conclusions

Er^{3+} on Al_2O_3-ZrO_2 powders was prepared by the solid-state reaction method at room temperature and studied by several characterization techniques for the understanding of their spectroscopic properties and adoption of a phase mixture (m-ZrO_2 and t-ZrO_2) at low Er^{3+} concentrations (3, 5, and 7 mol%). However, the t-ZrO_2 phase is dominant at high Er^{3+} concentrations (10 mol%) and shows high crystallinity. The analysis of the luminescence spectra of the excited $^2H_{11/2}/^4S_{3/2}$ and $^4F_{9/2}$ levels for ground state $^2I_{15/2}$ revealed changes in the non-radiative relaxation mechanism are responsible for the luminescence quenching. The luminescence in systems with low Er^{3+} concentrations shows the dominance of a green band over a red band. Chromaticity color coordinates indicate Er^{3+} ions in Al_2O_3-ZrO_2 systems enable the tuning of the emission color from orange to red through the control of the Er^{3+} concentration increase. The green and red bands at 567 and 683 nm exhibit lifetimes of up to 153.3 and 172.7 μs, respectively. Such a slightly shorter lifetime of $^4S_{3/2}$ can be attributed to the Er^{3+} concentration and surface defect.

References

[1] G. Blasse, B.C. Grabmaier, Luminescent Materials, Springer, Verlag Berlin Heidelberg, 1994.
[2] P.N. Prasad, Nanophotonics, Wiley, New York, 2004.
[3] C. Urlacher, C. Marco De Lucas, E. Bernstein, B. Jacquier, J. Mugnier, Study of erbium doped ZrO2 waveguides elaborated by a sol-gel process, Opt. Mater. Amst 12 (1999) 19–25.
[4] V.A.G. Rivera, F.A. Ferri, J.L. Clabel H., M.K. Kawamura, M.A. Pereira-da-Silva, L.A.O. Nunes, et al., High near-infrared emission intensity of Er 3+ -doped zirconium oxide films on a Si(100) substrate, Proc. SPIE 8621 (2013) 86211K.
[5] V.A.G. Rivera, Y. Ledemi, M. El-Amraoui, Y. Messaddeq, E. Marega, Green-to-red light tuning by up-conversion emission via energy transfer in Er3 +-Tm3 +-codoped germanium-tellurite glasses, J. Non. Cryst. Solids 392–393 (2014) 45–50.
[6] E.C.S.H.D.E. Harrison, N.T. McLamed, A new family of self-activated phosphors, J. Electrochem. Soc. 110 (1963) 23.
[7] S. Krishnan, C. Anderson, P. Nordine, Optical properties of liquid and solid zirconium, Phys. Rev. B 49 (1994) 3161–3166.
[8] J.E.P.-H. Ping Li, I. Wei Chen, X-ray-absorption studies of zirconia polymorphs. III. Static distortion and thermal distortion, Physic Rev. B 48 (1993) 10082.
[9] F.F. Lange, Transformation toughening, J. Mater. Sci. 17 (1982) 255–263.
[10] C. Ming, F. Song, F. Wang, S. An, Y. Cai, X. Ren, et al., Luminescent characters of Er 3 þ/Yb 3 þ co-doped ZrO 2 – Al 2 O 3 phosphors, J. Lumin 168 (2015) 59–61.
[11] R.I. Merino, J.A. Pardo, J.I. Peña, V.M. Orera, Microstructure-size dependence of the 1.520 μm Er[sup 3+] luminescence lifetime in Al[sub 2]O[sub 3]–ZrO[sub 2] eutectic melt growth composites, Appl. Phys. Lett. 80 (2002) 589.
[12] T. Rivera, R. Sosa, J. Azorín, J. Zarate, A. Ceja, Synthesis and luminescent characterization of sol-gel derived zirconia-alumina, Radiat. Meas. 45 (2010) 465–467.
[13] H. Schmalzried, Solid State Reactions, Verlag Chemie, Weinhein, FL, 1981.
[14] Q. Ding, S. Xiao, X. Yang, X. Zhang, Y. Xia, Z. Liu, Investigation of up-conversion luminescent properties of Er3+/Yb3+ co-doped ZrO2–Al2O3 powders, Opt. Mater. Amst 29 (2007) 773–777.
[15] J.S., F.F.B. Bondars, G. Heidemane, J. Grabis, K. Laschke, H. Boysen, Powder diffraction investigations of plasma sprayed zirconia, J. Mater. Sci. 30 (1995) 1621–1625.
[16] H.W. Smith, D.K. Newkirk Jr., The crystal structure of baddeleyite (monoclinic Zr O2) and its relation to the polymorphism of Zr O2, Acta Crystallogr. 18 (1965) 983.
[17] H. Tomaszewskp, K. Godwodb, Influence of oxygen partial pressure on the metastability of undoped zirconia dispersed in alumina matrix, J. Eur. Ceram. Soc. 15 (1995) 17–23.
[18] R.B.V.D.C.A. Larson, General Structure Analysis System — GSAS, Los Alamos National Laboratory, Los Alamos, USA, 2001.
[19] M. Zawadzki, D. Hreniak, J. Wrzyszcz, W. Mišta, H. Grabowska, O.L. Malta, et al., Photoluminescence and cathodoluminescence of Tb-doped Al2O3-ZrO2 nanostructures obtained by sol-gel method, Chem. Phys. 291 (2003) 275–285.
[20] A. Eichler, Tetragonal Y-doped zirconia: structure and ion conductivity, Phys. Rev. B 64 (2001) 174103.
[21] J.E.P.-H. Ping Li, I. Wei Chen, Characteristic local structures, Physic Rev. B 48 (1993) 10063–10073.
[22] N. Maeda, N. Wada, H. Onoda, A. Maegawa, K. Kojima, Spectroscopic properties of Er3+ in sol–gel derived ZrO2 films, Thin Solid Films 445 (2003) 382–386.
[23] G.S., A.P. Maciel, Influence of nanoenvironment on luminescence lifetime of Er 3+ -activated ZrO 2 nanocrystals, J. Opt. Soc.Am. B 21 (2004) 681–684.
[24] E.Y. Borovikova, V.S. Kurazhkovskaya, Infrared spectra and factor group analysis of vesuvianites in OH region, Vib. Spectrosc. 39 (2005) 95–98.
[25] J.L. Clabel H., V.A.G. Rivera, M. Siu Li, L.A.O. Nunes, E.R. Leite, W.H. Schreiner, et al., Near-infrared light emission of Er3+-doped zirconium oxide thin films: an optical, structural and XPS study, J. Alloys Compd. 619 (2015) 800–806.
[26] A.K. Singh, S.K. Singh, S.B. Rai, Role of Li + ion in the luminescence enhancement of lanthanide ions: favorable modi fi cations in host matrices, R. Soc. Chem. 9 (2014) 27039.
[27] P.K. Sharma, A.C. Pandey, G. Zolnierkiewicz, N. Guskos, C. Rudowicz, Relationship between oxygen defects and the photoluminescence property of ZnO nanoparticles: a spectroscopic view, J. Appl. Phys. 106 (2009) 094314.
[28] V.A.G. Rivera, Y. Ledemi, M.A. Pereira-da-Silva, Y. Messaddeq, E. Marega Jr., Plasmon-photon conversion to near-infrared emission from Yb3+: (Au/Ag-nanoparticles) in tungsten-tellurite glasses, Sci. Rep. 6 (2016) 18464.
[29] R.C., M.A.C.R.I. Merino, V.M. Orera, Characterization of point defects in yttria stabilized zirconia single crystals, J. Phys. Condens. Matter 3 (1991) 8491.
[30] R.R, J.F.P. Jenouvrier, M. Langlet, Influence of crystallisation on the photo-lumines- cence properties of Y2−xErxTi2O7 sol-gel thin film, Appl. Phys. A 77 (2003) 687.
[31] Z. Chen, W. Gong, T. Chen, S. Li, D. Wang, Q. Wang, Preparation and upconversion luminescence of Er3+/Yb3+ codoped Y2Ti2O7 nanocrystals, Mater. Lett. 68 (2012) 137–139.